Simultaneous Optical Speckle and ADONIS Imaging of the 126 mas Herbig Ae/Be Binary Star NX Puppis

W. BRANDNER [1], T. LEHMANN [2], M. SCHÖLLER [3], G. WEIGELT [3], H. ZINNECKER [4]

[1]*Astronomisches Institut der Universität Würzburg, Germany*
[2]*Universitätssternwarte Jena, Germany;* [3]*MPI für Radioastronomie, Bonn, Germany*
[4]*Astrophysikalisches Institut Potsdam, Germany*

Introduction

We have obtained simultaneous high spatial resolution optical speckle and near-infrared adaptive optics images of the 126 mas Herbig Ae/Be binary star NX Pup and could derive accurate estimates for the evolutionary status of both components. Furthermore, we were able to decompose the overall spectral energy distribution into its constituent parts, namely the contribution of the two stellar photospheres and the infrared excess due to circumstellar material associated with both stars.

The Herbig Ae/Be star NX Pup is located in the Gum nebula at a distance of ≈ 450 pc and belongs to a group of bright PMS stars which have been systematically monitored for more than a decade from La Silla in the course of the Long-Term Photometric Variables project (LTPV, Thé & Bibo, 1990, Sterken et al., 1995 and references therein).

On New Year's Day 1993, NX Pup was resolved as a binary with a separation of 126 mas by the Fine Guidance Sensors (FGS) of the Hubble Space Telescope (HST) in the V band (Bernacca et al., 1993). Exactly one year later (January 1st, 1994) the combined light of the close binary was decomposed from the ground for the first time using ESO's adaptive optics prototype COME-ON+ & SHARP in JHK at the ESO 3.6-m telescope (Brandner et al., 1995, see also Tessier et al., 1994 for details on the image reconstruction).

The combination of the optical HST data, calibrated in flux by interpolating LTPV observations, with the near infrared data obtained with COME-ON+ already allowed for a (crude) determination of the spectral types and luminosities, and hence masses and ages for both components. We could show that both stars are very likely pre-main se-
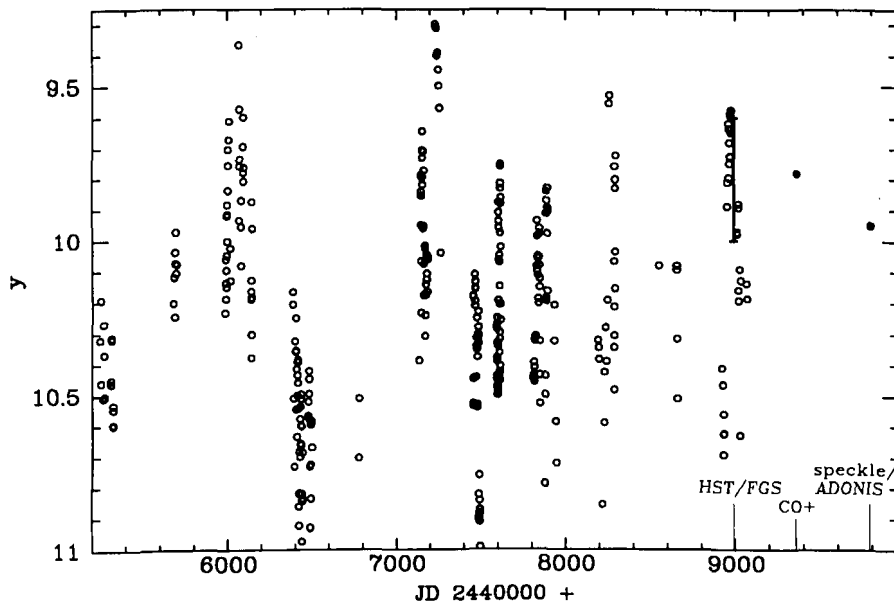

Figure 1: V (y in the Strömgren photometric system) light curve of NX Pup from 1983 to 1995 (compiled from LTPV data, open circles). Note the rapid variations with an amplitude of $\approx 1.7^m$. Marked are the dates of the HST/FGS observations, the first NIR adaptive optics observations (CO+), and the current simultaneous data set presented here. At the time of all three high angular resolution observations NX Pup was relatively bright.

quence stars exhibiting an IR excess and that the secondary has a spectral type between mid F and late G. However, by studying more than 350 individual Strömgren photometric measurements which had been accumulated in over 12 years of LTPV monitoring (cf. Fig. 1), we realised that a convergent picture of the evolutionary status of NX Pup A & B could only be obtained by quasi-simultaneous high spatial resolution observations in the optical and near infrared.

Observations

On March 11, 1995, three of La Silla's four largest optical telescopes (D1.54-m,

ESO/MPI 2.2-m, ESO 3.6-m) simultaneously observed NX Pup in the optical and in the near infrared utilising two of the most sophisticated high spatial resolution techniques – namely optical speckle in combination with speckle masking reconstruction (Weigelt, 1977) and adaptive optics imaging using ADONIS and the SHARP camera. We obtained simultaneous high spatial resolution images of NX Pup from the V to the K band (cf. Table 1).

The great drawback of all high spatial resolution instruments is their small field of view which makes it very time consuming to obtain absolute photometric calibrations by observing standard stars one by one. Therefore, it proved to be advantageous to have also a "smaller" telescope like the Danish 1.54-m with its "wide field" CCD camera (6' × 6' compared to 6" × 6" of the speckle camera) available for doing photometric calibrations while at the same time dedicating the larger telescopes to high-resolution imaging alone (a similar approach should be considered for forthcoming high spatial and high spectral resolution observations with the VLT, where flux calibrations could be obtained with an auxiliary telescope thus helping to in-

TABLE 1. Journal of observations (all observations are simultaneous within 3 hrs)

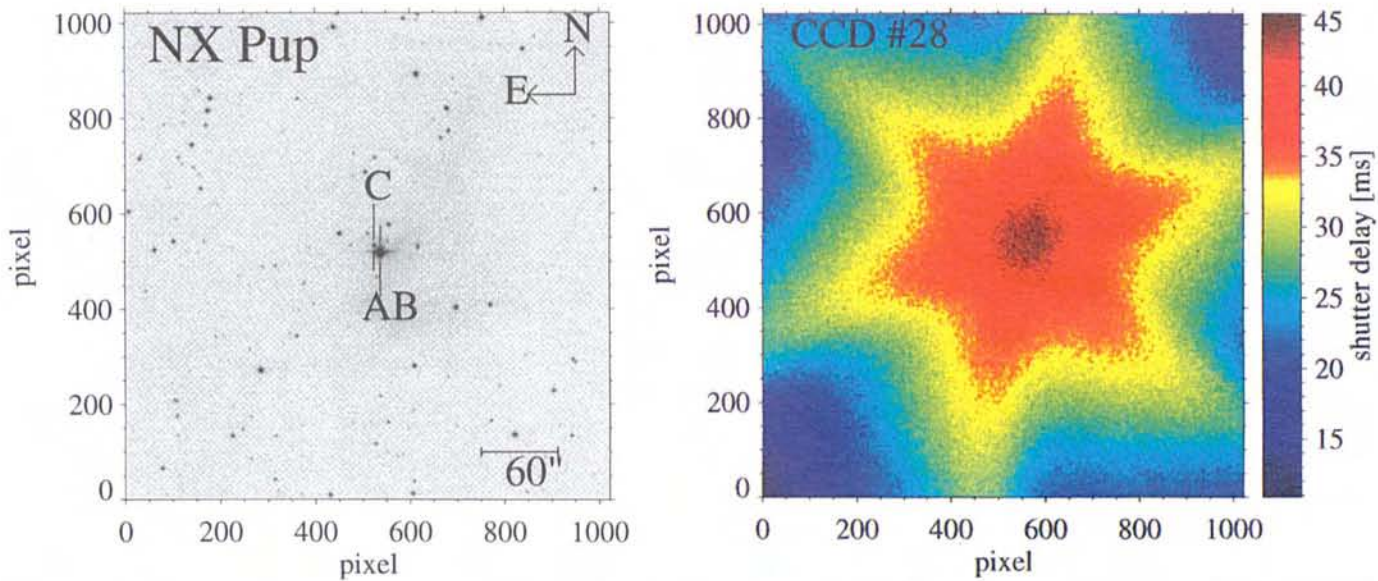| Telescope/instrument	UT (11.3.1995)	Filter (λ_c, FWHM)	Exposure time
D1.54/CCD camera	01:30	B,V,R	5s, 2s, 5s
ESO-MPG 2.2-m/speckle cam.	01:15	V (545 nm, 30 nm)	629×50 ms
ESO-MPG 2.2-m/speckle cam.	00:15, 03:00	R (656 nm, 60 nm)	1927×70 ms
ESO-MPG 2.2-m/speckle cam.	01:00, 02:45	R (656 nm, 30 nm)	2285×70 ms
ESO-MPG 2.2-m/speckle cam.	03:15	Hα (656.3 nm, 4 nm)	1903×70 ms
ESO 3.6-m/ADONIS+SHARP	02:30	H, K	400×0.5 s (each)

Figure 2: 1.5-s R exposure of the region around NX Pup obtained with the CCD camera at the D1.54-m telescope in 1995 March 11 (left). NX Pup AB (unresolved) and the associated classical T Tauri star NX Pup C are marked. The shutter delay in the central part of the CCD amounts to 45 ms, which in the 1.5-s exposure image induces a photometric error of 3%. The corresponding shutter map is shown on the right.

crease the efficiency of the larger telescopes and to improve the scientific quality of the data).

Data Reduction

Photometric calibration of short-exposure CCD images: shutter maps

All CCD cameras at ESO are equipped with a mechanical shutter. Problems in short exposures (< 10 s) arise from the shutter delay, i.e. the time delay between starting or ending an exposure by sending a signal to the CCD camera and the actual beginning of the shutter movement. Furthermore, mechanical shutters need a certain time to move from the centre of a CCD to its edge and vice versa. The resulting (inhomogeneous) illumination pattern on the CCD leads to gradients across the field and to photometric errors. Mapping the shutter movement yields a typical delay between 50 ms (CCD camera at D1.54-m) and 500 ms (EMMI/Red at the NTT) for the central part of the CCD, which in a 1-s exposure already amounts to a photometric error of 5% to 50%!

This is well known, and the usual advice given to observers to circumvent this problem is not to take exposures shorter than 10 s. However, when observing bright objects (e.g. CCD standard star fields) with a larger telescope, one is forced to defocus the telescope in order to avoid saturation of the brightest stars on the CCD. This in turn induces errors in the photometric transformations for the (usually not defocused) programme stars.

A better approach is to actually map the shutter movement and the resulting illumination pattern on the CCD. The

procedure to obtain such a shutter map is straightforward: a series of short-long-short exposures, typically domeflats with exposure times of = 0.5 s (ts) and 3 s (tl) and count rates of a few 1000 ADU (short) to less than 20,000 ADU (long) are repeated eight to ten times. After averaging the two short exposures of each series, the resulting shutter map can be computed by

$$\text{shutter map} = (\text{short} \times \text{tl} - \text{long} \times \text{ts}) / (\text{long} - \text{short})$$

where "short" and "long" are the raw data (i.e. bias subtracted but not flat-

fielded) and "ts" and "tl" are the exposure times of the short and the long exposure, respectively.

The resulting shutter map for the CCD camera at the Danish 1.54-m is shown in Figure 2[1]. A comparison of shutter maps obtained several months apart indicate a stability to within 10%. Hence, residual photometric errors for a 1-s scientific ex-

---

[1] Shutter maps for the CCD cameras at the Dutch 90-cm and the Danish 1.54-m, and EFOSC2 at the ESO/MGP 2.2-m are available via WWW from http://www.astro.uni-wuerzburg.de/~brandner/ shuttermaps.html. Shutter maps for EMMI (red & blue) and SUSI will be made available by the NTT team in the near future.
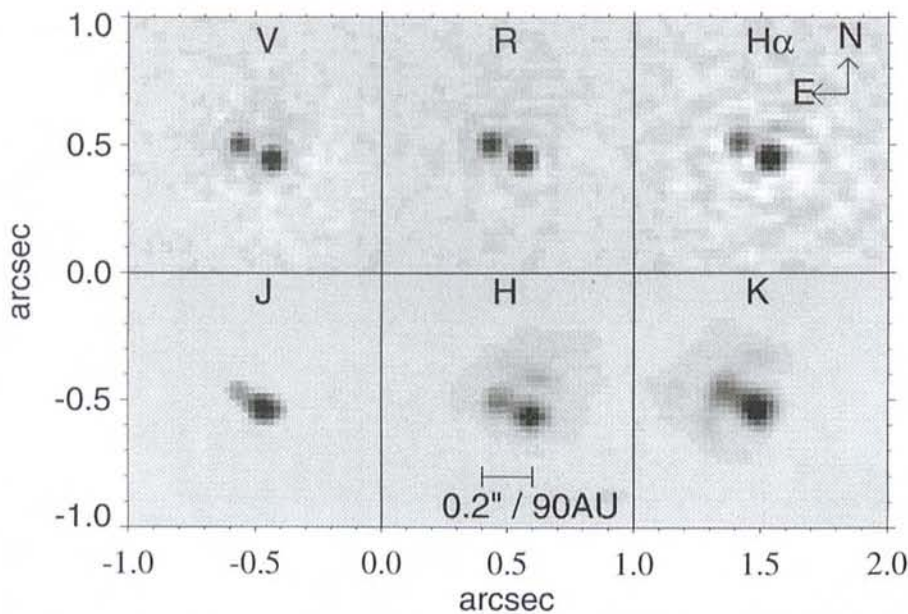

Figure 3: Set of simultaneous high spatial resolution images of NX Pup A and B. The optical data (top) have been obtained with a speckle camera at the ESO/MPI 2.2-m, whereas the near-infrared data have been obtained with ADONIS/SHARP at the ESO 3.6m telescope. The speckle data allow for the determination of the spectral type of the NX Pup B and reveal that the majority of the Hα excess originates in NX Pup A which is also the component with the stronger IR excess.
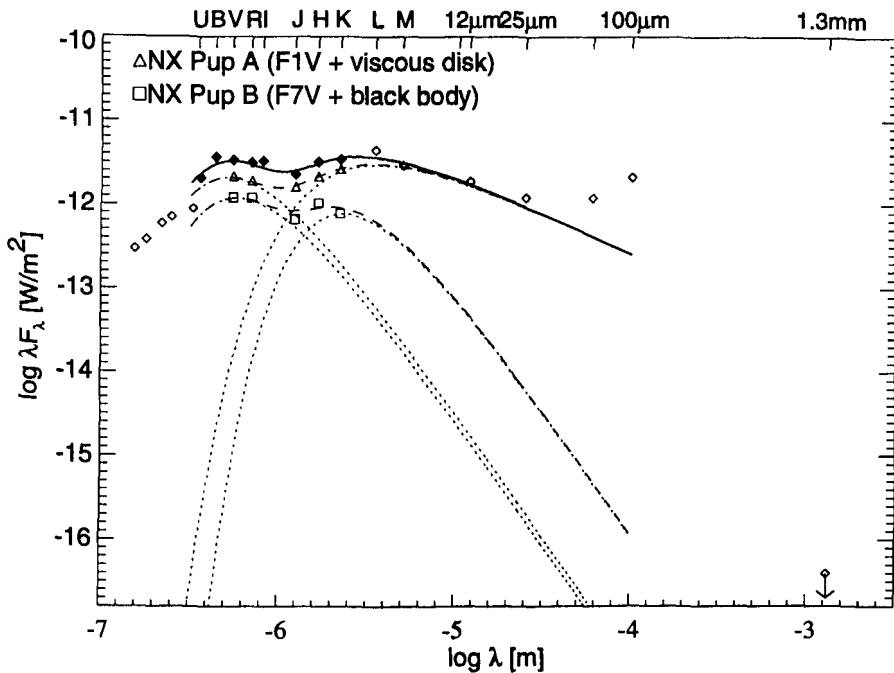
UBVRI J H K L M   12μm25μm   100μm   1.3mm

Figure 4: Dereddened (assuming $A_v = 0.48^m$) spectral energy distribution λF_λ of NX Pup A and B from the UV to the mm range. The filled diamonds, open triangles, and open squares indicate our own simultaneous measurements. The total spectral energy distribution can be decomposed into four parts (dotted lines): the photospheric emission from NX Pup A (F1V) and NX Pup B (F7V), a viscous accretion disk around NX Pup A, and circumstellar matter around NX Pup B which is approximated by a blackbody. The dashed lines mark both the SEDs of the individual stellar photospheres plus the IR excess due to circumstellar matter for NX Pup A and B. The overall SED is indicated by a solid line and gives a reasonable fit to the observed flux distribution (diamonds).

Table 2: *Evolutionary status of NX Pup A & B.*

NX Pup	A	B
Separation	0".126 ± 0".003	
PA	62°.8 ± 1°.7[a]	
SpT	F0–F2	F7–G4
$L/L_\odot$	16–19	7–9
Mass	≈ 2 $M_\odot$	1.6–1.9 $M_\odot$
Age	$3–5 \times 10^6$ yr	$2–6 \times 10^6$ yr

posure can be reduced from 10% to 1% even with shutter maps not obtained in the same night. All short exposure CCD images (observations of CCD standard star fields and of NX Pup) were corrected using the shutter map.

Speckle and adaptive optics observations

The speckle images were reconstructed by the speckle masking method (Schöller et al., 1996). The flux calibration was done by combining the relative photometry of the components derived from the speckle images with the absolute photometry of the (unresolved) components obtained with the Danish 1.54-m telescope.

The adaptive optics images were processed following the procedure described by Tessier et al. (1994). IR standard stars were observed with ADONIS/SHARP to allow for a flux calibration.

Results

Most of the light detected in V and R is emitted by the stellar photospheres of NX Pup A and B. Both components also exhibit a NIR excess. While the SED of NX Pup B peaks at H, the SED of NX Pup A is still rising at K. Hence, the majority of the IR excess arises from component A.

The photometric variability has been studied extensively by Bibo & Thé (1991). We reanalysed the colour magnitude relations derived from the LTPV data and found indications that variable extinction is the main cause for the variability. The blueing in colours when NX Pup is near its minimum brightness can be explained by additional scattered light due to circumstellar material (see Schöller et al., 1996).

If we adopt a MK type of F1 IV–V for NX Pup A, the observed V–R colour (0.30^m) yields a visual extinction $A_v \approx 0.48^m$. By assuming the same extinction for NX Pup B, its V–R colour yields a spectral type F7V. However, the fact that NX Pup B's IR excess is significantly smaller than that of NX Pup A might indicate that, while it suffers the same foreground extinction as NX Pup A, its circumstellar extinction might be considerably less. Studies, e.g. by Krautter (1980), indicate that the amount of foreground extinction in the direction of the Gum nebula might be as small as $A_v \approx 0.15^m$ out till 500 pc from the Sun. If NX Pup B suffered no additional extinction, its V–R colour would yield a spectral type of G4V. Accordingly, we compute $L_{bol} \approx 7.3 – 9.4 \, L_\odot$. Mass and age determinations based on theoretical evolutionary tracks computed by D'Antona & Mazzitelli (1994) are summarised in Table 2.

The IR excess of NX Pup A can be approximated by a viscous accretion disk spectrum in which F_λ falls off $\propto \lambda^{-4/3}$ towards longer wavelengths. The non-

detection of 1.3 mm dust continuum emission (Henning et al., 1994) suggests that the disk around NX Pup A is cut off at about 20 AU possibly due to the presence of component B which itself has much less circumstellar matter left.

In a future observing run we aim at obtaining high spatial resolution observations of NX Pup near its minimum brightness. One would expect that NX Pup A then is completely obscured and would only be visible in the optical though light scattered by circumstellar material, similar to the active Herbig Ae/Be star Z CMa, where the IR companion was detected in the visual e.g. by Barth et al. (1994). Measurements of the polarisation of NX Pup A & B near minimum brightness using speckle polarimetry would be a test for the scattered light hypothesis.

Clearly, for both NX Pup A and B spatially resolved imaging towards longer wavelengths are necessary, which in turn allow for more detailed model calculations and to better constrain the structure and geometry of the circumstellar material around each star. With the equivalent of TIMMI in combination with adaptive optics at one VLT telescope it will become possible to resolve NX Pup also in the L and M, whereas the VLTI will allow high spatial resolution observations of NX Pup at 10 and 20 microns.

References

Barth W., Weigelt G., Zinnecker H. 1994, *A&A* **291**, 500.

Bernacca P.L., Lattanzi M.G., Bucciarelli B. et al. 1993 *A&A* **278**, L47.

Bibo E.A., Thé P.S. 1991, A&AS **89**, 319.

Brandner W., Bouvier J., Grebel E.K., et al. 1995 *A&A* **298**, 818.

D'Antona F., Mazzitelli I. 1994, ApJS **90**, 467.

Henning Th., Launhardt R., Steinacker J., Thamm E. 1994, *A&A* **291**, 546.

Krautter, J. 1980, *A&A* **89**, 74.

Schöller M., Brandner W., Lehmann T., Weigelt G., Zinnecker H. 1996 *A&A* submitted.

Sterken C., Manfroid J., Beele, D., et al. 1995 *A&AS* **113**, 31.

Tessier E., Bouvier J., Beuzit J.-L., Brandner W. 1994 *The Messenger* **78**, 35.

Thé P.S., Bibo E. 1990 *The Messenger* **61**, 39.

Weigelt G. 1977, *Optics Commun.* **21**, 55.

E-mail address: Wolfgang Brandner, brandner@astro.uni-wuerzburg.de